[10]R. A. Ferrell, Rev. Mod. Phys. 28, 308 (1956).
[11]J. P. Carbotte, Phys. Rev. 155, 197 (1967).
[12]B. Bergersen and J. H. Terrell, *Soft X-Ray Band Spectra*, edited by D. J. Fabian (Academic, London, 1968), p. 351.
[13]H. L. Weisberg and S. Berko, Phys. Rev. 154, 249 (1968).
[14]P. Kubica, B. T. A. McKee, A. T. Stewart, and M. J. Stott (unpublished).

PHYSICAL REVIEW B VOLUME 5, NUMBER 6 15 MARCH 1972

Optical Properties of Rb between 3.3 and 10.5 eV*

U. S. Whang† and E. T. Arakawa
Health Physics Division, Oak Ridge National Laboratory, Oak Ridge, Tennessee 37830
and
T. A. Callcott‡
Physics Department, University of Tennessee, Knoxville, Tennessee 37916
(Received 13 September 1971)

The optical and dielectric constants of Rb have been determined from reflectance measurements for photons of energy between 3.3 and 10.7 eV. Reflectance measurements were made as a function of incident angle at a Rb-substrate interface in an ultrahigh-vacuum system. The refractive index (n) was determined from the critical angle for total internal reflection, and the absorption coefficient (k) from the slope of the reflectance curve at the critical angle. The real part of the dielectric function (ϵ_1) and the optical conductivity ($\sigma = \omega\epsilon_2/4\pi$) were derived from n and k. In σ, we find a broad strong peak centered at 7 eV. It is attributed to absorption processes involving plasmon-assisted interband transitions and to direct interband transitions to "f" bands. ϵ_1 is analyzed in terms of a nearly-free-electron model to obtain a value for the contribution of core polarization to ϵ_1 of $4\pi m_0\alpha = 0.25 \pm 0.02$, and an effective mass of $m_{\text{eff}} = (1.03 \pm 0.02)m_0$.

INTRODUCTION

The alkalis are the simplest of the metals, in that their properties most nearly match those predicted using a simple nearly-free-electron (NFE) model of metals. Optical measurements on Na, K, Rb, and Cs in the visible and infrared region give results in generally good agreement with the NFE model.[1,2] These results and optical measurements on Na at higher energies suggest that there may be additional absorption above the plasma frequency that cannot be accounted for by the absorption mechanisms usually included in the NFE model.[3] We have recently reported measurements of the optical and dielectric constants of Cs for photon energies between 4 and 10 eV that conclusively demonstrate the existence of such an additional absorption process in this material.[4,5] A broad absorption peak with a maximum at 5 eV was found in the optical conductivity which we interpreted as absorption resulting from the simultaneous excitation of a collective mode and an interband transition.

In this paper we report experimental determinations of the index of refraction (n), the absorption coefficient (k), the real part of the dielectric response function (ϵ_1), and the optical conductivity (σ) for Rb for photon energies of 3.3–10.7 eV. A broad peak centered at 7 eV is observed in the conductivity. The peak is somewhat weaker and broader and lies at a higher energy than the corresponding peak found for Cs. A Kramers-Kronig analysis applied to the imaginary part of the dielectric response function ($\epsilon_2 = 4\pi\sigma/\omega$) is used to calculate the effect of the interband transitions and of the broad high-energy absorption peak on ϵ_1. These contributions are subtracted from ϵ_1 so that the remaining portion represents the ϵ_1 expected for a NFE model containing only free-carrier absorption. This corrected value of ϵ_1 is used to obtain values of the core polarization and the effective mass, which are the adjustable parameters of such a free-electron model. The values obtained are compared with those obtained by other authors.

EXPERIMENTAL PROCEDURES

The basic experimental procedures used in this work have been described in detail elsewhere.[3,5] The sample chamber is shown schematically in Fig. 1. In brief, Rb was deposited on the flat surface of a transparent semicylinder substrate. The reflectance of light incident on the Rb film through the substrate was measured as a function of angle. A semicylinder is used so that incident and re-

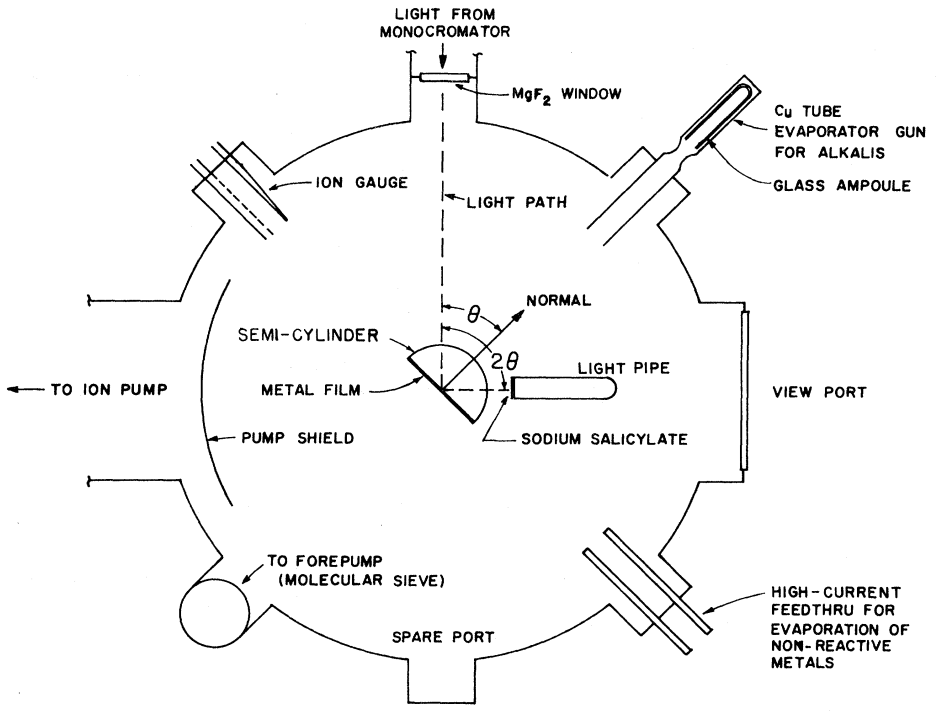

FIG. 1. Sample chamber for reflectance measurements.

flected beams pass through the vacuum-substrate interface at normal incidence for all reflection angles. The sample holder and light-pipe detector are connected through a gear mechanism which rotates the light path through twice the angle of the sample and thus keeps the face of the light pipe in the reflected beam throughout the experiment. The system presently in use differs from those described earlier[3–5] in that it is an ion-pumped ultrahigh-vacuum system with gearing for the angle doubler mounted inside the experimental chamber rather than a diffusion-pumped system with external gearing.

Semicylinders of quartz, CaF_2, and MgF_2 were used as substrates. Reproducible results were obtained only with carefully cleaned substrates. Quartz was cleaned by methods described in our earlier paper on Cs.[5] MgF_2 and CaF_2 were cleaned with procedures described by Sowers *et al.*[6] The glass-light-pipe detector was coated with sodium salicylate to obtain sensitivity in the vacuum ultraviolet. Its output was monitored through a window by a photomultiplier mounted outside the chamber.

Glass ampoules containing about 0.5 g of 99.8% Rb under vacuum were mounted in an evaporation gun consisting of a length of OFHC Cu tubing attached to the chamber through a Cu flange gasket and sealed off at the other end by an inert-gas weld. Following a pumpdown procedure which included a system bake of 200 °C and a bakeout of the evaporation gun at 400 °C (a temperature above its operating temperature during evaporation), the system typically reached a vacuum of 5×10^{-10} Torr as measured by a nude ion gauge mounted in the wall of the sample chamber. The glass ampoule was then broken by squeezing the Cu tube, and the system pumped until it returned to the 10^{-10}-Torr range. By heating the Cu gun externally, Rb films of $\gtrsim 20\,000$-Å thickness were deposited on water-cooled substrates in 3–5 min. Pressures during evaporation were in the 10^{-7}-Torr range and returned to around 2×10^{-9} Torr shortly after evaporation was complete. This pressure was maintained for several hours but increased slowly with time to about 10^{-7} Torr. The relatively high pressures result from the high vapor pressure of Rb at room temperature. Consequently, the residual gas in the vacuum was mostly Rb vapor with much lower partial pressures of other gases. The films obtained were specularly reflecting at the substrate-film interface and somewhat frosty at the free surface. The frosty surface was composed of small crystallites that grew slowly in size over a period of several days. Experimental curves of reflectance as a function of angle [$R(\theta)$ curves] made on Rb at the Rb-substrate interface were unchanged after many hours.

Rb was deposited on only half of the substrate surface. The remaining half was used as a reference surface having a substrate-vacuum inter-

face. $R(\theta)$ curves made at the vacuum interface gave values of the total incident beam intensity and of the index of refraction of the substrate that were used in the subsequent analyses.

$R(\theta)$ curves were taken between angles of 5° and 84°. At angles less than 5° the incident beam was blocked by the light pipe and at angles greater than 84°, by the mounting structure of the semicylinder.

DETERMINATION OF OPTICAL CONSTANTS

The optical constants were determined from the $R(\theta)$ curves near the critical angle for total internal reflection. If the index of refraction of the metal, n, is less than that of the transparent substrate, n_s, and the absorption coefficient is zero, the critical angle is given by

$$n_{rel} = n/n_s = \sin\theta_c \,. \tag{1}$$

If the relative-absorption coefficient, defined as $k_{rel} = k/n_s$, is small but not zero, the relative index of refraction may be obtained from θ_m, the angle of maximum slope of the $R(\theta)$ curve. For $k_{rel} \leq 0.02$, to 1% accuracy

$$n_{rel} = \sin\theta_m \,. \tag{2}$$

Hunter has calculated the small corrections to the above equation that allow its use for all values of k_{rel} up to about 0.2.[7] In all cases where $0 < n_{rel} < 1$ and $k_{rel} < 0.1$, n may be obtained from θ_m to within about a 2% uncertainty by using Hunter's corrections.

We have shown in an earlier paper that the slope of the $R(\theta)$ curve at θ_m depends strongly on the value of the absorption coefficient k_{rel} but very weakly on n_{rel} and the polarization.[5] In particular, for $0.2 \leq n_{rel} \leq 1$ and $0.02 \leq k_{rel} \leq 0.12$, the slope of $R(\theta)$ at θ_m determines the value of k_{rel} within 5% regardless of the value of n_{rel}. The explicit dependence of k_{rel} on slope for a large range of n_{rel} and polarizations will be discussed in a separate paper.[8] Using these curves and Hunter's calculations, one can determine n and k from the angular position of θ_m and the magnitude of the slope of $R(\theta)$ at this angle without reference to the remaining portions of the $R(\theta)$ curves.

It is, of course, possible to make a least-squares fit of $R(\theta)$ at all angles to obtain n and k. We found that only for the MgF_2 substrate did the values thus obtained agree closely with values obtained by measuring θ_m and the slope at θ_m. The problem was traced to the fact that at angles beyond the critical angle the shape of the experimental curves differed from that expected theoretically. The effect is shown in Fig. 2, where $R(\theta)$ at 3523 Å for Rb on MgF_2, CaF_2, and quartz are plotted. The point of maximum slope is marked by circles on the three curves. The horizontal displacement of θ_m for the three curves results from the different indices of refraction of the substrates. Values of n and k obtained from θ_m and the slope at θ_m are the same for all curves within our limits of error ($n = 0.41$, $k = 0.17$). But only for the MgF_2 substrate does the theoretical $R(\theta)$ curve generated from these n and k values closely match the experimental curve at angles beyond the critical angle. $R(\theta)$ curves for the other substrates are depressed and flattened above these angles. The deviations from ideal $R(\theta)$ curves result from effects occurring at the interface, but the details are unknown. We conclude that values of n and k determined by fitting the slope of the curve at θ_m are more reliable than those obtained by fitting the entire curve, and that in our experiments the $R(\theta)$ curves obtained for MgF_2 substrates are the most reliable over the full range of angles measured.

Values of n and k obtained from several films on a MgF_2 substrate are shown in Fig. 3. The solid line in this figure gives the averaged values of n and k which were used in all further analyses. Above 1500 Å, k values show scatter of about 5% around the average value. At shorter wavelengths when $k < 0.05$, the scatter increases to some 20%. Values of n remain within 3% of the average over the entire range of wavelengths measured.

For wavelengths between 1100 and 3000 Å, values of n and k determined by the angle-and-slope method from data from other substrates scatter about the same average values as the data from MgF_2 alone. At longer wavelengths, systematic deviations occur that are substrate dependent. For reasons discussed above, we think that the values ob-

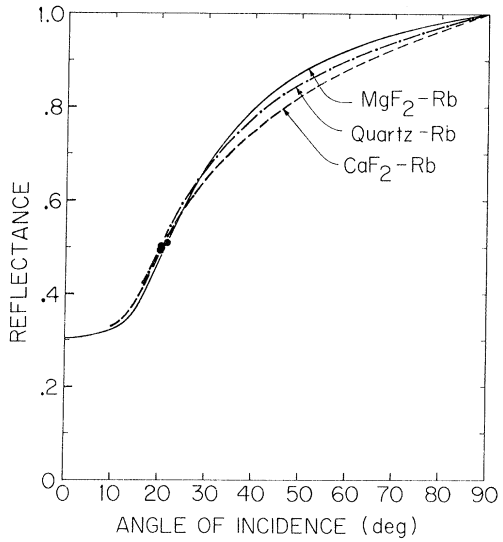

FIG. 2. Dependence of reflectance curve on the surface condition of the substrate. Solid, dash-dot, and dashed lines are reflectances obtained from MgF_2-, quartz-, and CaF_2-Rb interfaces, respectively.

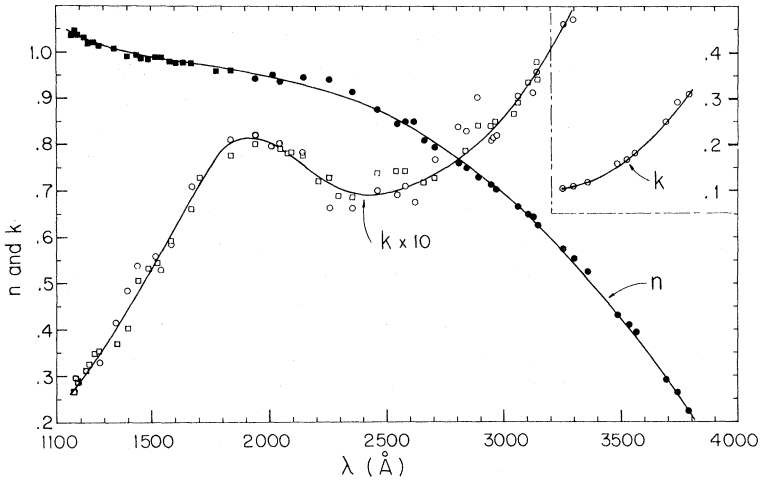

FIG. 3. Experimental values of n and k obtained from the films on the MgF_2 substrate. Solid and open squares are n and k values, respectively, obtained from the critical-angle method. Solid and open circles are those values calculated by computer from the data curve of $R(\theta)$ vs θ.

tained with MgF_2 substrates are the most accurate.

Table I gives averaged values of n, k, ϵ_1, ϵ_2, and σ obtained from our data.

ANALYSIS AND DISCUSSION

The optical conductivity given by $\sigma = \omega\epsilon_2/4\pi = nk\omega/2\pi$ is plotted in Fig. 4. The dominant feature is a strong broad peak centered at about 7 eV. We emphasize that data from all substrates gave this peak in nearly identical form. The small, rather sharp peak near 3.5 eV is substrate dependent, being largest for CaF_2 and smaller for MgF_2 and quartz. It seems probable that it is associated with some surface effect. The data shown as open squares at energies below 4 eV are those obtained by Smith using an ellipsometric technique.[2] The data shown as closed circles are data of Aufschnaiter[9] obtained from ellipsometry, and the equilateral triangles are data of Ives and Briggs[10] obtained from reflection measurements. It is interesting to note that the values of Ives and Briggs are very close to those that we obtained when using a CaF_2 substrate. From our experience it seems probable that surface effects can play a large role in determining the optical constants measured in the interband absorption region of Rb. Smith's data are probably most reliable in the low-energy region. It clearly shows the contribution of interband transitions to the absorption between 1 and 3 eV. For this reason and because it matches our own data in the region of overlap, we will refer to his work when it is necessary to use low-energy data in the following discussion.

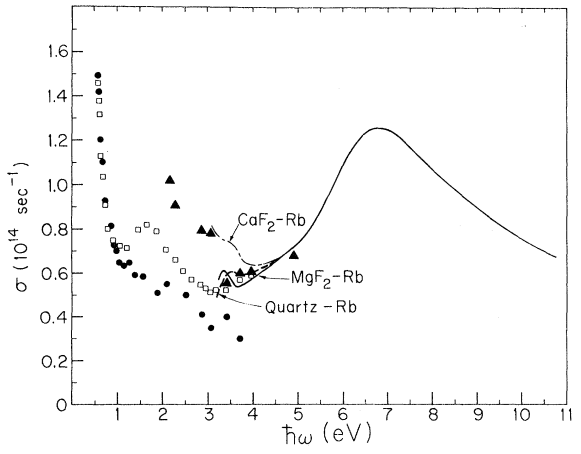

FIG. 4. σ vs $\hbar\omega$ of Rb. Solid line is the curve obtained from the averaged smooth curve of n and k using MgF_2 substrate. Squares, closed circles, and equilateral triangles are data points obtained by Smith, by Aufschnaiter, and by Ives and Briggs, respectively.

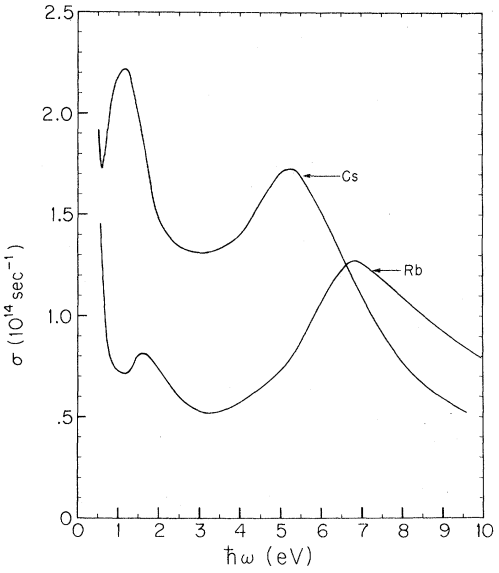

FIG. 5. σ vs $\hbar\omega$ of Rb and Cs.

TABLE I. Optical and dielectric constants of Rb.

λ (Å)	E (eV)	n	k	ϵ_1	ϵ_2	σ (10^{14} sec^{-1})
1165	10.64	1.041	0.027	1.08	0.056	0.72
1192	10.40	1.03	0.028	1.07	0.059	0.74
1218	10.18	1.03	0.030	1.06	0.062	0.76
1235	10.04	1.02	0.031	1.05	0.064	0.78
1254	9.89	1.02	0.033	1.04	0.067	0.80
1280	9.69	1.02	0.035	1.04	0.071	0.83
1320	9.39	1.01	0.038	1.03	0.076	0.87
1351	9.18	1.01	0.040	1.02	0.081	0.90
1399	8.86	1.00	0.044	1.01	0.089	0.95
1462	8.48	0.997	0.050	0.992	0.099	1.02
1520	8.16	0.990	0.055	0.977	0.108	1.07
1543	8.04	0.988	0.057	0.973	0.112	1.09
1578	7.86	0.985	0.060	0.967	0.118	1.12
1606	7.72	0.983	0.062	0.962	0.123	0.15
1636	7.58	0.980	0.065	0.956	0.128	1.17
1670	7.43	0.978	0.068	0.952	0.133	1.20
1700	7.29	0.976	0.071	0.948	0.139	1.22
1780	6.97	0.970	0.077	0.935	0.150	1.27
1837	6.81	0.965	0.080	0.925	0.155	1.28
1875	6.61	0.962	0.081	0.919	0.156	1.25
1942	6.39	0.955	0.081	0.905	0.155	1.20
2015	6.15	0.947	0.080	0.890	0.152	1.13
2044	6.07	0.944	0.079	0.885	0.150	1.10
2145	5.78	0.932	0.076	0.863	0.141	0.98
2214	5.60	0.928	0.073	0.856	0.135	0.92
2305	5.38	0.908	0.071	0.819	0.128	0.84
2400	5.17	0.891	0.069	0.789	0.123	0.77
2461	5.04	0.877	0.070	0.764	0.122	0.74
2544	4.87	0.855	0.070	0.726	0.120	0.71
2613	4.75	0.837	0.072	0.695	0.120	0.69
2750	4.51	0.790	0.075	0.618	0.119	0.65
2889	4.29	0.739	0.080	0.535	0.118	0.61
3000	4.13	0.697	0.086	0.478	0.120	0.60
3105	3.99	0.648	0.093	0.411	0.121	0.58
3256	3.81	0.570	0.106	0.314	0.121	0.56
3359	3.59	0.510	0.119	0.246	0.121	0.54
3434	3.61	0.465	0.136	0.198	0.126	0.55
3563	3.48	0.385	0.179	0.116	0.138	0.58
3620	3.43	0.350	0.211	0.078	0.148	0.61
3695	3.35	0.293	0.258	0.019	0.151	0.62
3740	3.32	0.262	0.292	0.003	0.153	0.62
3800	3.26	0.216	0.346	−0.073	0.149	0.59

We may distinguish at least three different contributions to the conductivity. Below about 1 eV, free-carrier absorption processes dominate. Direct interband excitations between the filled conduction band and the next-higher unfilled band produce absorption between 1 and 3 eV. Both of these absorption processes may be understood in terms of the NFE model and have been studied extensively both experimentally and theoretically.[1,2,11-14] The slow rise in σ between 3 and 5 eV and the broad strong peak between 5 and 10 eV with a maximum near 7 eV are much more difficult to explain. As an aid in the discussion of this peak, we plot σ for both Rb and Cs in Fig. 5. The low-energy data are Smith's. The high-energy peak in Rb is slightly weaker and broader and is centered at higher energy than the comparable peak in Cs. The intensity ratio of the high-energy peak to the interband peak is greater in Rb than in Cs, however.

The question of greatest interest is whether the absorption can be understood in terms of one-electron transitions or whether it must be explained by a many-body theory in terms of the excitation of collective modes. Within the framework of one-electron theory, interband excitations from the conduction band to "*d*" or "*f*" bands can contribute to absorption in this energy range. According to Kenney's calculations, the *d*-like bands are strongly mixed with *p*-like states in Rb and lie at energies 2–4 eV above the conduction-band states.[15] The *f* bands lie at energies 5–9 eV above the conduction-band states. It is thus energetically possible that transitions to *f* bands are responsible for the higher-energy peak. Two factors argue against this interpretation. It is difficult to understand the greater relative strength of the high-energy peak as compared to the interband peak at 2 eV on this basis. Transition probabilities between *s*-like conduction-band states and high-lying *f*-band states are expected to be very much smaller than those between filled conduction-band states and the next-higher band. This factor should more than compensate for the higher density of states of the *f* bands. Moreover, the similar peak observed in Cs is not located at an energy where absorption can be conveniently explained by transitions to *f* bands. It falls at an energy between the calculated *d* bands and *f* bands where very few final states are available. Neither of these arguments is completely conclusive. The experimentally determined peak magnitudes may be in error; in our work, data taken in the visible region have been particularly susceptible to distortion by surface effects. The band-structure calculations we have used may be in error. Finally, to our knowledge the absorption expected from transitions to *f* bands has not been calculated in realistic fashion.

The second possible explanation of the peak at 7 eV involves a many-body absorption process which produces a final state consisting of a plasmon plus an electron-hole pair. Other possible many-body effects were discussed in the Cs paper[5] and eliminated from consideration. Those arguments remain valid here. This explanation was favored in the case of Cs where calculated *f* bands were at too high an energy to account for the absorption peak. Lundqvist and Lyden[16] and Janow and Tzoar[17] have applied many-body theory to simple models to calculate the optical absorption from such processes. Lundqvist and Lyden predict an absorption peak with a threshold at the plasmon energy plus the threshold energy for interband transitions, and a maximum at approximately the plasmon energy plus the energy of the interband peak. On this basis, the threshold for Rb would be near 4 eV and the peak maximum about 5 eV. The experimental peak maximum is at 7 eV. The qualitative agreement for Cs is much better, since the theory of Lundqvist and Lyden predicts a peak at about 5 eV in agreement with our experimental data. The calculation of Lundqvist and Lyden also predicts a magnitude for

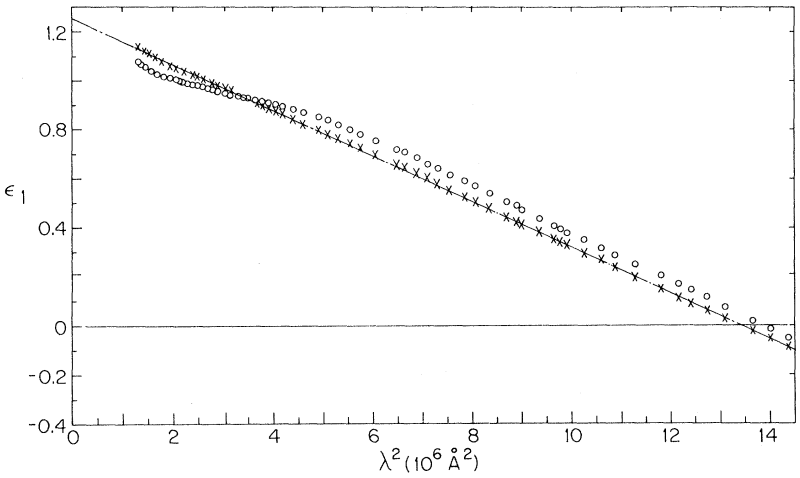

FIG. 6. ϵ_1 vs λ^2. Circles are the points obtained from the smooth curve of n and k values. Crosses are a plot of $\epsilon_1 - \delta\epsilon_1$, the free-carrier contribution to ϵ_1.

absorption due to such "plasmon-assisted transitions" that is approximately 50% of that due to direct transitions. For Rb, this is in conflict with the relative magnitudes of the interband peak at 2-eV and the 7-eV peak. Again the arguments are not conclusive, since a very simple model was used in these calculations. Even so, it is disturbing that the relative magnitudes of the interband and high-energy peaks are not approximately the same for both Cs and Rb, since it can be shown that the same transition matrix elements are included in both the interband transition and the many-body process of Lundqvist and Lyden. We think that a conclusive explanation of our data will require further calculations within the framework of both one-electron and many-body theory. Neither of the mechanisms discussed above seems to account for the relative magnitudes of the interband in high-energy peaks in Rb.

The real part of the dielectric function, ϵ_1, is plotted as a function of wavelength squared in Fig. 6. The open circles are points calculated directly from n and k using the relation $\epsilon_1 = n^2 - k^2$. Since $n \gtrsim 10k$ over most of the range of interest, ϵ_1 is known with approximately the same accuracy as n.[2] The analysis of ϵ_1 for Rb follows closely that previously applied to data from Cs.[5] We present here a somewhat abbreviated version of the discussion given there.

The plot of ϵ_1 vs λ^2 may be compared with results obtained by Cohen using an NFE model,[11] where

$$\epsilon_1 = 1 + 4\pi n_0 \alpha_0 - (\omega_a/\omega)^2 + \delta\epsilon_1(\omega) \,. \tag{3}$$

Here α_0 is the core polarizability, which is constant in this frequency range, n_0 is the number of atoms per unit volume, and ω_a is related to the effective mass m_a of the conduction electrons through the expression

$$\omega_a^2 = 4\pi n_0 e^2/m_a \,. \tag{4}$$

In Cohen's formalism, $\delta\epsilon_1(\omega)$ includes contributions to ϵ_1 from interband transitions. It may equally well include the effect on ϵ_1 of all absorption processes except the free-carrier Drude term, whose effect is included in the other terms of Eq. (3).

$\delta\epsilon_1(\omega)$ may be calculated from ϵ_2 (or σ) using the Kramers-Kronig relation

$$\delta\epsilon_1(\omega') = \frac{2}{\pi}\int_0^\infty \frac{\omega\delta\epsilon_2(\omega)}{\omega^2 - \omega'^2}\, d\omega \,, \tag{5}$$

where $\delta\epsilon_2(\omega)$ represents the contribution of all processes except free-carrier absorption to ϵ_2. In practice, $\delta\epsilon_2$ was obtained from the expression $\delta\epsilon_2 = 4\pi\delta\sigma/\omega$, where $\delta\sigma(\omega)$ are experimental values of the conductivity from which the contribution of free-carrier absorption has been subtracted. The free-carrier absorption was characterized by fitting a Drude term to Smith's data below 1 eV. This Drude absorption term was characterized by a damping constant of $2\pi\gamma\hbar = 0.025$ eV and the plasma energy of 3.40 eV obtained below. At energies above 10 eV, $\delta\sigma$ was extrapolated smoothly to zero at 30 eV. There will be another absorption peak at an energy of about 14.5 eV resulting from excitation from core levels.[18] The existence of such an absorption peak will only slightly affect our analysis of data at photon energies below 10 eV because of the resonant energy denominator of the Kramers-Kronig relation. When $\delta\epsilon_1$ is subtracted from ϵ_1, the remaining portion represents the ϵ_1 expected for an NFE model containing only free-carrier absorption. In Fig. 6 values of $\epsilon_1 - \delta\epsilon_1$ are plotted as crosses. The solid line is the best straight-line fit to the crosses. From the slope and intercept of the straight line, we obtain the following values for the NFE parameters:

$$4\pi n_0 \alpha = 0.25 \pm 0.02 \,,$$

$$m_a = (1.03 \pm 0.02)\, m_0 \,,$$

TABLE II. NFE parameters from optical data.

	$\hbar\omega_{p,\mathrm{eff}}$ ($\epsilon_1 = 0$)	$\hbar\omega_p$ ($\epsilon_1 - \delta\epsilon_1 = 0$)	m_a/m	$4\pi n_0 \alpha$
Present work (uv)	3.33 ± 0.03	3.40 ± 0.03	1.03 ± 0.02	0.25 ± 0.02
Smith (infrared) (Ref. 2)	...	3.40	1.16	(0.11)
Smith (visible-uv)	(3.40)	3.40	(1.07)	(0.20)
Aufschnaiter (infrared) (Ref. 9)	3.39	...	1.28	(0.01)
Aufschnaiter (visible-uv)	3.04	3.04	1.21	0.33
Ives and Briggs (visible-uv) (Ref. 10)	3.01	...	1.08	0.50

where m_0 is the free-electron mass.

In Table II our results are compared with those obtained by other workers using optical measurements at lower photon energies. Included also are values of the effective plasma energy $\hbar\omega_{p,\mathrm{eff}}$, defined as the energy for which $\epsilon_1 = 0$, and plasma energies $\hbar\omega_p$ obtained from the intercept of $\epsilon_1 - \delta\epsilon_1$ with the λ^2 axis. Numbers in parentheses were calculated by us from the published data.

Our value of the effective plasma energy agrees well with that obtained by Kunz[19] (3.39 eV) from electron-energy-loss measurements. Our value of effective mass is comparable with those obtained by fitting the data of Smith and of Ives and Briggs in the visible and ultraviolet. However, in Rb, as in Cs, consistently higher effective masses are found by fitting the data in the infrared. This seems to be a real effect, found in the data of all workers, that needs an explanation. It is suggestive that the same plasma energy is obtained by fitting ϵ_1-vs-λ^2 data above and below the plasma energy but that the slope, and hence the effective mass, changes. It may be that many-body-dressing effects change in the vicinity of the plasma energy and that different effective masses are appropriate in the two regions.

Our value of core polarization is comparable with values obtained recently from visible and ultraviolet data by other workers. It is more accurate, however, since it results from fitting data much closer to the $\lambda = 0$ intercept. It agrees well with the value of 0.28 that may be calculated from values of atomic polarizabilities of alkali ions in the alkali halides.[11,20] The lower values obtained from an extrapolation of infrared data result from the smaller slope, and higher effective mass, that must be used to fit the data below the plasma energy.

ACKNOWLEDGMENTS

The helpful discussions with Dr. R. H. Ritchie and Dr. R. N. Hamm of the Oak Ridge National Laboratory and B. I. Lundqvist of Chalmers University of Technology in Sweden concerning various theoretical aspects of the problem are gratefully acknowledged.

*Research sponsored by the U. S. Atomic Energy Commission under contract with Union Carbide Corporation.

†Research Assistant, National Science Foundation Grant No. GP 11917, University of Tennessee, Knoxville, Tenn. 37916.

‡Consultant, Oak Ridge National Laboratory.

[1]H. Mayer and B. Hietel, in *Optical Properties and Electronic Structure of Metals and Alloys*, edited by F. Abelès (North-Holland, Amsterdam, 1966).

[2]N. V. Smith, Phys. Rev. B2, 2840 (1970).

[3]J. C. Sutherland, R. N. Hamm, and E. T. Arakawa, J. Opt. Soc. Am. 59, 1581 (1969).

[4]U. S. Whang, E. T. Arakawa, and T. A. Callcott, Phys. Rev. Letters 25, 646 (1970).

[5]U. S. Whang, E. T. Arakawa, and T. A. Callcott, J. Opt. Soc. Am. 61, 740 (1971).

[6]B. L. Sowers, E. T. Arakawa, and R. D. Birkhoff, J. Chem. Phys. 54, 2319 (1971).

[7]W. R. Hunter, J. Opt. Soc. Am. 54, 15 (1964).

[8]U. S. Whang, R. N. Hamm, T. A. Callcott, and E. T. Arakawa (unpublished).

[9]S. von Aufschnaiter, thesis (Bergakademie Clausthal University, Berlin) (unpublished).

[10]H. E. Ives and H. B. Briggs, J. Opt. Soc. Am. 27, 395 (1937).

[11]M. H. Cohen, Phil. Mag. 3, 762 (1958).

[12]P. N. Butcher, J. Phys. A 64, 765 (1951).

[13]A. O. E. Animalu, Phys. Rev. 163, 557 (1967); Phys. Rev. B2, 282 (1970).

[14]L. W. Beeferman and H. Ehrenreich, Phys. Rev. B 2, 364 (1970).

[15]J. F. Kenney, MIT Solid State and Molecular Theory Group Quarterly Progress Report No. 66, 1967 (unpublished).

[16]B. I. Lundqvist and C. Lyden, in *Proceedings of the Electronic Density of States Symposium* (U. S. GPO, Washington, D. C., 1959), p. 50.

[17]R. Janow and N. Tzoar, Bull. Am. Phys. Soc. 15, 368 (1970).

[18]R. G. Oswald and T. A. Callcott, Phys. Rev. B 4, 4122 (1971)

[19]C. Kunz, Z. Physik 196, 311 (1966).

[20]J. R. Tessman, H. Kahn, and W. Shockley, Phys. Rev. 92, 890 (1953).